IEEE Access
Multidisciplinary | Rapid Review | Open Access Journal

Received 27 August 2023, accepted 24 September 2023, date of publication 29 September 2023, date of current version 9 October 2023.

Digital Object Identifier 10.1109/ACCESS.2023.3320936

RESEARCH ARTICLE

Development of an Equivalent Electronic Circuit Model for PEMFC Voltage Based on Different Input Electrical Currents

ÁNGEL HERNÁNDEZ-GÓMEZ[1], DIEGO LANGARICA-CORDOBA[1], (Senior Member, IEEE), PANFILO R. MARTINEZ-RODRIGUEZ[1], (Senior Member, IEEE), DAMIEN GUILBERT[2], VICTOR M. RAREZ-RIVERA[3,4], AND BELEM SALDIVAR[5]

[1]School of Sciences, Universidad Autónoma de San Luis Potosí (UASLP), San Luis Potosí 78295, Mexico
[2]Group of Research in Electrical Engineering of Nancy (GREEN), Université de Lorraine, 54000 Nancy, France
[3]Department of Renewable Energy, Centro de Investigación Científica de Yucatán (CICY), Mérida, Yucatán 97205, Mexico
[4]CONACYT, Mexico City 03940, Mexico
[5]Department of Automatic Control, CINVESTAV-IPN, Mexico City 07360, Mexico

Corresponding author: Diego Langarica-Cordoba (diego.langarica@uaslp.mx)

This work was supported by Consejo Nacional de Ciencia y Tecnología (CONACYT), Mexico, through the Project "Control Design Strategies and Transformerless Power Converters for PVS" under Grant 319541.

ABSTRACT The technological development and exploration of the proton exchange membrane fuel cell have relied on several mathematical models. However, despite the wide variety of models, the equivalent electronic circuit model is the most suitable for describing electrical behavior, designing electronic interfaces, and analyzing control and reliability strategies. In addition to the fact that this type of model is scarce to model the fuel cell voltage, an equivalent electronic circuit model that depends only on the input current has not been reported (in general, the reported mathematical models take into account additional variables such as humidity, temperature, pressure, etc.). For this reason, this work focuses on developing an equivalent electronic circuit model for the fuel cell voltage that depends only on the input current. Besides, the configuration of the proposed circuit (one voltage source, two capacitors, and three resistors) is simpler than the circuits proposed in previous works. To validate the model and its parameters, current tests from 1.2 kW Nexa® fuel cell power module were used. The comparison between the experimental data and the developed model confirms the efficiency of the equivalent electronic circuit model to reproduce the fuel cell voltage as a function of the current.

INDEX TERMS Adaptive parameters, circuit electronic modeling, fuel cell voltage, proton exchange membrane fuel cell.

I. INTRODUCTION

Concern about greenhouse gas emissions and the problems of fossil fuel consumption has led to the search for renewable energy sources, which aim at being sustainable with affordable prices, highly efficient, and with low environmental impact in energy conversion. Therefore, interest in power generation systems such as Fuel Cell (FC) has increased in recent years. FC systems are clean, environmentally friendly, and sustainable energy sources due to their higher energy density, energy efficiency, and low emissions [1], [2].

The main operation of the FC is to transform gaseous fuel chemical energy into electricity. FCs can be used as an alternative stationary and mobile power source [3], [4]. Today different manufacturers offer many options and types of FC. They can be classified according to their specific characteristics, such as the type of fuel used, the reaction temperature, and the electrochemical material used [5]. The main FCs reported in the literature are Proton Exchange Membrane (PEMFC), direct methanol, solid oxide, molten

The associate editor coordinating the review of this manuscript and approving it for publication was Paolo Crippa.

carbonate, phosphoric acid, alkaline, and microbial [6], [7]. In the field of both stationary and mobile applications, PEMFCs are among the most widely used and promising. This is due to their many advantages, which are quick and silent start-up operation, robustness, and a relatively low operating temperature ranging from 20 to 80 ^{o}C [8].

For the development of PEMFC systems, mathematical modeling is a powerful tool for simulation, exploration of control strategies, prediction, and understanding of power generation system behavior [9], [10], [11]. A wide variety of models that can be classified as 0-D to 3-D models [12], empirical and semi-empirical models [13], analytical models [14], statistical physics-based models [15], [16], and performance and fault diagnosis models [17], [18] have been developed. The models that are most suited to the purpose of a microgrid or electrical emulator development are the equivalent Electronic Circuit Models (ECM) since these models allow describing the electrical behavior of the PEMFC or how it interacts with power conditioning circuits such as converters and other connected electrical systems [19]. In addition, ECM are a powerful tool for electronic interface design and control as well as for the development of reliability test analysis [20], [21]. Two types of ECM have been reported: dynamic models and passive models [19]. A dynamic model takes into account both chemical and thermodynamic processes. Thus, it is possible to understand the unique characteristics of the PEMFC (i.e. a clear understanding of various factors including additional losses due to ripple current) to implement the best system in terms of efficiency and cost [22], [23]. Furthermore, a dynamic model can be used to optimize the performance, transient response, and efficiency of power converters, so that suitable control systems can be designed to meet the load demand [22], [24]. With a passive model, it is possible to determine the performance and degradation of the PEMFC while in standby mode. This mode applies to uninterruptible power systems where the PEMFC is idle most of the time and reliability is paramount [19].

The first ECM has been proposed by Larminie et al. [25]. In this first model, the electrodes are each represented by a capacitor in parallel with a resistance and a voltage potential. For the development of ECM, some authors relied on mathematical models that describe the behavior of PEMFC, taking into account several variables that influence the behavior of PEMFC voltage [26], [27], [28], [29]. Other authors have chosen to describe the polarization curve taking into account the behavior of the electronic components [22], [24], [30]. In [31], the electrochemical behavior of a PEMFC has been taken into consideration for the development of an ECM and a Matlab-Simulink® model has been established. The authors in [32] used the equivalent double-layer capacitor to avoid step-transient voltage variations. This capacitor has been optimized based on the transient phase convergence and its lifetime. In [33], a state space model of a PEMFC DC/DC converter system has been presented. This model describes the relation between different electrical variables and can be applied to any FC operating point. The authors in [34] presented a simplified and novel dynamic ECM for PEMFC suitable for power system analysis and design. In [35], both the PEMFC and the stacks have been tested under various operating conditions to identify the variations of the model parameters and thus be able to carry out a more detailed analysis of the processes that occur in a PEMFC through the ECM. In [36], an easy-to-use digital simulator for PEMFC based on an ECM using a LabVIEW® power supply has been presented. The authors in [37] modeled the open-circuit output voltage, voltage losses, mass balance, and thermodynamic energy balance of a PEMFC, along with the formation of the charge double layer at the cathode. In [38], an ECM based on double-layer charge dynamics has been developed assuming a dielectric relaxation of the material to represent dynamic processes in the typical frequency range of the inverter current ripple. In [39], ECM parameters have been estimated based on impedance data sets obtained through electrochemical impedance spectroscopy (EIS) processes. In these processes, a small magnitude alternating current sweeping a wide spectrum of frequencies has been superimposed on a direct current drawn from the PEMFC while the resulting voltage response is measured, which helps to understand the effects of current ripple on the PEMFC while operating with power conditioning units. In [40], an ECM has been developed focused on PEMFC voltage and temperature distribution. The developed model detects, identifies, and simulates different PEMFC failures. In [41], the authors built an ECM based on analogies that allow a uniform representation of electrical, pneumatic, and thermal transients. Furthermore, it has been shown how models representing different transients can be coupled as part of a PEMFC system. In [42], the authors developed an ECM to describe the static-dynamic behavior of the PEMFC stack under pulsed loads up to frequencies of 10 kHz. Thus, with this model, it is possible to perform dynamic simulations of power electronic systems directly connected to the PEMFC stack without the need to parameterize with special EIS measurements. In [43], an electrically controllable ECM for PEMFC is developed and implemented in MATLAB®. In addition, the authors presented a method to parameterize the models developed in MATLAB-Simulink® through experimental results. The authors in [44] applied an ECM to fit the EIS measurements of laser coating samples measured at open circuit potential. The diagram of the circuit for this ECM takes into consideration the resistance of the solution, the charge transfer resistance at the electrolyte interface, and the Warburg resistance. In [45], a new diagnostic technique has been developed to determine the hydration of the PEMFC using an ECM. In this case, the electronic circuit proposed by Fouquet et al. [46] was used. The authors in [47] made a review of PEMFC emulators, in which it is shown how the development and construction of emulators for PEMFC voltage is related to ECM. In addition, this work shows

TABLE 1. Main characteristics of the ECM proposed in recent years.

Reference	ECM variables	ECM components	PEMFC model
[31]	Current Temperature Pressure	3 resistors 1 capacitor 1 voltage source	500 W BCS stack
[32]	Current Temperature Pressure	3 resistors 1 capacitor 1 voltage source	600 W stack
[33]	Current Temperature Pressure	2 resistors 1 capacitor 1 voltage source	Ballard Nexa
[34]	Current Temperature Pressure	4 resistors 1 capacitor 1 voltage source	1.2 kW Nexa power module
[35]	Current Temperature Pressure	3 resistors 2 capacitors 1 voltage source	ITAE-CNR PEMFC
[36]	Current Temperature Pressure	3 resistors 1 capacitor 1 voltage source	Relion SR-12 500 W stack
[37]	Current Temperature Pressure	3 resistors 1 capacitor 1 voltage source	500 W stack
[38]	Current Temperature	3 resistors 3 voltage sources	14 KW commercial Morphic
[39]	Current Pressure	4 resistors 3 capacitors 1 voltage source	1.2 kW Nexa power module
[40] [43]	Current Temperature Pressure	3 resistors 1 capacitor 1 voltage source	A single PEMFC
[41]	Current Temperature Pressure	3 resistors 1 capacitor 1 voltage source	500 W SR-12 Avista Labs
[42]	Current Temperature Pressure	3 resistors 2 capacitors 1 voltage source	2 kW Stack
[44] [45] [46]	Current Temperature	4 resistors 3 capacitors 1 voltage source	A single PEMFC
Proposed ECM	Current	3 resistors 2 capacitors 1 voltage source	1.2 kW Nexa power module

examples of electronic circuit designs based on ECM. Table 1 shows the main characteristics of the ECM proposed in recent years (i.e., the variables that have been taken into account for the development of the ECM, the electronic components used in the PEMFC equivalent circuit, and the type of PEMFC used for the development and validation of the ECM).

As can be seen in Table 1, despite the different models proposed, ECM that depends solely on the input current has not been reported. For this reason, this paper makes the following contributions:

- Development of an ECM for the PEMFC voltage that depends only on the input current. The proposed ECM holds significant potential in facilitating a comprehensive analysis, designs, optimal sizing, and efficient control strategies for power converters integrated with PEMFC systems.
- An electronic circuit diagram composed of one voltage source, two capacitors, and three resistors, which can be built quickly and cheaply to emulate a PEMFC for prototyping purposes.

To validate the model and its parameters, five different PEMFC current tests of a 1.2 kW Nexa® PEMFC power module were considered; three increasing and two decreasing currents. Finally, the results of the statistical tests applied to the simulated and experimental data confirmed the efficiency of the ECM to reproduce the PEMFC voltage as a function of the current. Therefore, with the mathematical model developed in this work, it is possible to easily build an electronic circuit for PEMFC voltage emulation.

This work is divided into five sections. After providing the current state-of-the-art and motivations to carry out this work in the Introduction, Section II aims at presenting the PEMFC technology and describes the experiment that was carried out to collect voltage and current data. Then, in Section III, the ECM for PEMFC voltage is provided. In Section IV, the ECM parameters are calculated. In Section V, the ECM is experimentally validated by using data from a 1.2 kW Nexa® PEMFC power module. Besides, a discussion is provided to summarize and comment on the obtained results. Finally, some concluding remarks are given in Section VI.

II. PEMFC TECHNOLOGY: FEATURES AND MODELING ISSUES

A. FEATURES OF PEMFC

A considerable amount of research work has been carried out to develop highly efficient and reliable PEMFCs for use in various applications such as portable and stationary. Significant development has been achieved recently, especially in materials and current density, which will eventually lead to increased power density and make the device more efficient and reliable [48]. In addition, PEMFCs have higher efficiency compared to heat engines and in their use in modular electricity generation [3].

A PEMFC consists of a proton exchange membrane sandwiched between two electrodes (anode and cathode). The membrane has a special property that allows protons to pass through while blocking electrons. Hydrogen gas passes over the anode and, with the help of a catalyst, separates into electrons and hydrogen protons. The protons flow to the cathode, through the proton exchange membrane while the electrons flow through an external circuit, thus creating electricity. The hydrogen protons and electrons combine with oxygen flow through the cathode to produce water, see Fig. 1.

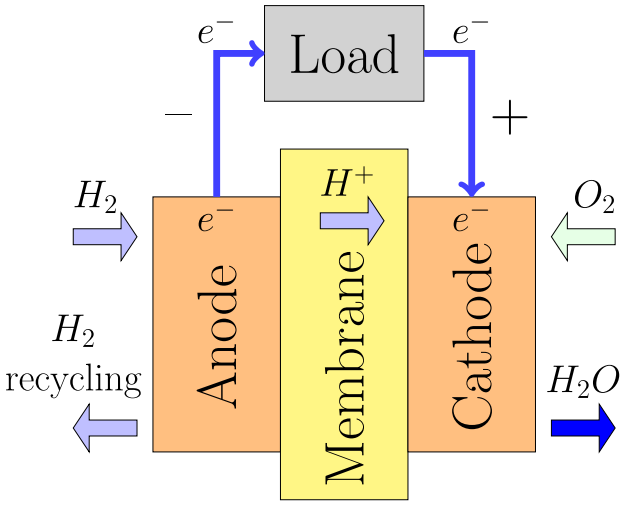

FIGURE 1. Schematic diagram of a basic PEMFC.

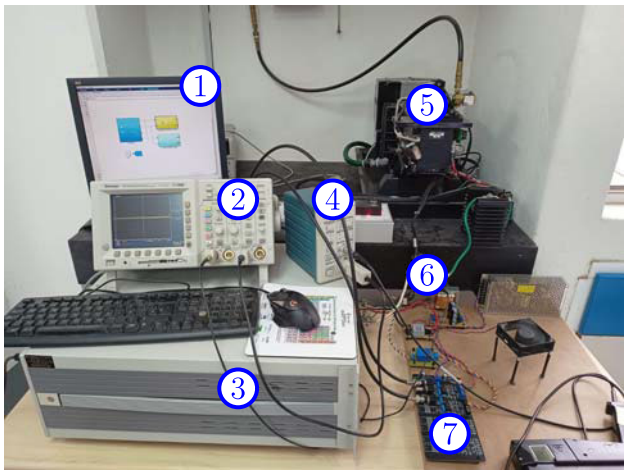

FIGURE 2. Experimental test bench using 1.2 *kW* Nexa® PEMFC power module (Manufacturer Ballard) [50].

The reactions in the PEMFC are [37]:

$$\begin{aligned} 2H_2 &\rightarrow 4H^+ + 4e^- \text{ (anode reaction)} \\ O_2 + 4H^+ + 4e^- &\rightarrow 2H_2O \text{ (cathode reaction)} \\ 2H_2 + O_2 &\rightarrow 2H_2O \text{ (overall reaction)} \end{aligned} \quad (1)$$

Typical characteristics of PEMFC can be identified in a polarization curve, which is a plot of cell current versus cell voltage. As more current is drawn from the FC, the voltage drops due to the electrical resistance of the fuel cell, inefficient transport of reactant gas, and slow reaction rate. Since lower voltage indicates lower fuel cell efficiency, low-load operation is preferred. However, this will increase the volume and weight of the fuel cell. Furthermore, the constant low-load operation is not practical in mobile applications where frequent load changes are required. The polarization curve varies with different operating conditions, including pressure, temperature, partial pressure of reactants, and membrane humidity [3]. As is shown in Fig. 1, to form a complete FC system, the PEMFC stack requires several auxiliary components and four main flow subsystems: the hydrogen supply system to the anode; the air supply system to the cathode; the humidifier and the cooler that maintain the humidity degree, and the temperature of the PEMFC. Reactant flow rate, total pressure, reactant partial pressure, membrane temperature, and humidity are the main parameters that need to be regulated to avoid constant warm-ups and ensure fast system transient response, safe shutdown, system robustness, and an adaptation to power changes. The main control devices are the compressor motor for airflow and pressure regulation, the hydrogen flow and pressure regulation valve, the water pump for temperature regulation, and the humidifier for humidity control. It is worth mentioning that changes in one parameter influence the others [3], [49]. Thus, this is the cause of a PEMFC being a complex system.

B. EXPERIMENTAL DATA RECORDING

The data for this research was taken from a 1.2 *kW* Nexa® PEMFC power module (manufacturer Ballard) [50]. This equipment is a fully automated, compact, and low-maintenance PEMFC stack that provides a power output of 1.2 *kW* at a voltage of 24 *V*. Besides, this module incorporates a protection diode to prevent reverse current from entering the FC stack, see Fig. 2. Unfortunately, this diode exhibits an undesirable power dissipation, resulting in a reduction of effective output power to approximately 1 *kW*. The output voltage ranges from an open circuit voltage of 42 *V* to a fully loaded voltage of 22 *V*. The nominal output voltage is 26 *V* with a nominal load current of 46 *A*. The specifications of the studied commercial 1.2 *kW* Nexa® PEMFC power module are provided in Table 2. The experimental set-up consisted of the following components:

(1) Computer with Matlab® software and DSPACE DS1103 data acquisition system.
(2) Digital oscilloscope for monitoring.
(3) Electronic load.
(4) Current amplifier probe.
(5) A 1.2 *kW* Nexa® PEMFC power module
(6) Voltage source, LV25P voltage sensor, CSNE151 current sensor.
(7) Op-amp signal conditioning circuit.

The experiment consisted of observing the behavior of the PEMFC voltage using five different input current tests. The results of this experiment are shown in Fig. 3.

The five current tests were monotonic (tests 1 to 3 consider a current increase from no load to a given maximum current, and tests 4 to 5 consider a current decreasing behavior, from a maximum current to no-load operation), which allows studying the behavior of voltage and power (polarization curve) when the PEMFC is subjected to this type of input current. Notice that the hysteresis band exhibited by the

TABLE 2. Specifications of 1.2 *kW* Nexa® PEMFC power module (manufacturer Ballard) [50].

Power	Rated net power	1200 *W*
	DC voltage range	22–50 *V*
	Rated voltage	26 *V*
	Rated current	46 *A*
Fuel	Purity	$\geq$ 99.99% H_2 (vol)
	Pressure	0.7–17 *bar* (10–250 *PSIG*)
	Consumption	$\leq$ 18.5 *SLPM*
Emissions	Water	$\leq 870\ mL \cdot hr^{-1}$
	Noise	$\leq 72\ dBA \cdot m$
Physical	Length	56 *cm* $\times$25 *cm* $\times$ 33 *cm*
	Weight	13 *kg* (29 *lbs*)

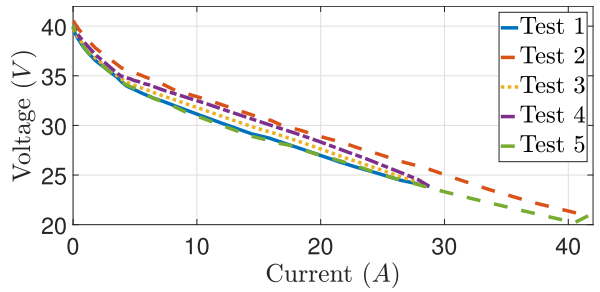

FIGURE 3. PEMFC voltage behavior with five different input current tests.

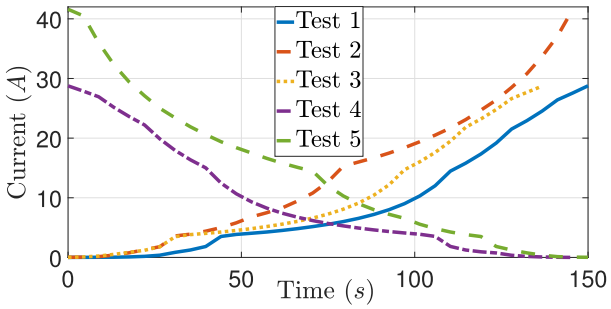

FIGURE 4. Behavior of PEMFC current tests as a function of time.

TABLE 3. Main characteristics of the five experimental tests.

Test	Final time	Max. current	Min. voltage	Max. voltage
Test 1	150.0 *s*	28.7732 *A*	23.8637 *V*	39.9558 *V*
Test 2	145.6 *s*	41.6000 *A*	20.8900 *V*	40.5000 *V*
Test 3	136.8 *s*	28.7216 *A*	23.8637 *V*	39.7628 *V*
Test 4	145.6 *s*	28.7607 *A*	23.8637 *V*	39.9127 *V*
Test 5	150.0 *s*	41.6000 *A*	20.2000 *V*	40.1000 *V*

PEMFC voltage presents a complex nonlinear behavior that is difficult to model, therefore it is out of the scope of this work. All tests started with an experimental time of zero. Besides, the three increasing tests had a current initial value of zero while for both decreasing tests the current final value was zero as illustrated in Fig. 4. The main characteristics of each experimental test (i.e. final time, maximum current, minimum voltage, and maximum voltage) are shown in Table 3.

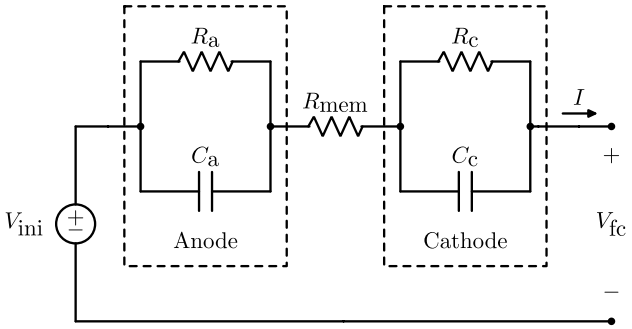

FIGURE 5. Electronic circuit sketch for PEMFC voltage.

After obtaining the experimental data from the PEMFC, a V-I relation was observed. It is noted that when the electric current increases the voltage decreases, and in the same way, when the current decreases the voltage increases. Besides, when developing the model, it has been taken into consideration that the voltage and current in a cell have a maximum (polarization curve). This proposed model only depends on the input current and is explained in detail in the next section.

III. EQUIVALENT ELECTRICAL CIRCUIT AND MATHEMATICAL MODELING

As it is widely known, the PEMFC voltage V_{fc} can be expressed in terms of the Nernst's voltage E_{th} and of the three main types of voltage drops; ohmic V_{ohm}, activation V_{act}, and concentration V_{con} [51], [52].

$$V_{fc} = E_{th} - V_{ohm} - V_{act} - V_{con}. \tag{2}$$

This equation represents a static model of the PEMFC voltage. This static model has been used by many authors as reported in the literature [53], [54]. However, in [40], the authors assumed the PEMFC as an electronic circuit to develop a static-dynamic ECM. This work is inspired by the ECM proposed in [40], wherein the double-layer charging effect serves as the main regulator of the PEMFC voltage dynamics. In this work, the capacitance property was used to model the double layer that corresponds to the electrolyte/electrode contact since it functions as a storage of electrical charges. Also, for the activation and concentration voltages, a voltage change requires a charge time (in case of voltage increase) or a leakage period (in case of voltage decrease). It is important to note that the ohmic voltage drop is not influenced by any time delay as it changes instantly. The equivalent electrical circuit is sketched in Fig. 5.

The equivalent circuit model is composed of the following elements:

- Two resistance-capacitor branches to model the dynamics both at the anode and cathode (activation and concentration voltage drops $\eta_{act} + \eta_{con}$):

$$\eta_{act} + \eta_{con} = \eta_{act,c} + \eta_{con,c} + \eta_{act,a} + \eta_{con,a}, \tag{3}$$

where the dynamic equations for $\eta_{act,c} + \eta_{con,c}$ and $\eta_{act,a} + \eta_{con,a}$ are:

$$\frac{d\left(\eta_{act,c} + \eta_{con,c}\right)}{dt} = \frac{1}{C_c} \cdot I - \frac{1}{\tau_c} \cdot \left(\eta_{act,c} + \eta_{con,c}\right), \tag{4}$$

$$\frac{d\left(\eta_{act,a} + \eta_{con,a}\right)}{dt} = \frac{1}{C_a} \cdot I - \frac{1}{\tau_a} \cdot \left(\eta_{act,a} + \eta_{con,a}\right), \tag{5}$$

where I is the PEMFC current, C_c and C_a are the capacitors for cathode and anode, respectively. The electrical time constants τ_c and τ_a governing the dynamics are variables according to the operating conditions at the input of the PEMFC.

- One resistance to model the membrane (ohmic voltage drop η_{ohm}):

$$\eta_{ohm} = I \cdot R_{mem}, \tag{6}$$

where R_{mem} is an internal resistance in the circuit.

- A DC voltage source V_{ini} to model the Nernst's voltage:

$$V_{ini} = E_{th}. \tag{7}$$

The equivalent resistances R_c and R_a are determined based on the activation voltage and input current of the PEMFC, also they are related with τ_c and τ_a, respectively, see (8) and (9) [55], [56], [57].

$$\tau_c = C_c \cdot R_c = C_c \cdot \left(\frac{\eta_{act,c} + \eta_{con,c}}{I}\right), \tag{8}$$

$$\tau_a = C_a \cdot R_a = C_a \cdot \left(\frac{\eta_{act,a} + \eta_{con,a}}{I}\right). \tag{9}$$

So, the equivalent static-dynamic model for the PEMFC voltage can be expressed as:

$$V_{fc}(t) = V_{ini} - I(t) \cdot R_{mem} - \eta_{act}(t) - \eta_{con}(t). \tag{10}$$

IV. PARAMETER ESTIMATION

In this section, the parameters of (10) are estimated. To adequately estimate the parameters, the five different PEMFC current tests (I_i, where i takes the value between 1 and 5) were analyzed. Each test I_i was estimated using Matlab® Curve Fitting Application. Among all the functions available in this application, the function with the best fit for each I_i was the Fourier series of 4 terms, see (11).

$$I_i(t) = a_{i,0} + \sum_{j=1}^{4} \left(a_{i,j} \cdot \cos[w_i \cdot t] + b_{i,j} \cdot \sin[w_i \cdot t]\right). \tag{11}$$

Table 4 shows the different values of the parameters for the Fourier series of each current test I_i.

Fig. 6 and 7 illustrate the behavior of the five current tests and the behavior of their corresponding Fourier series. Fig. 6 shows the behavior of the three tests of increasing current while Fig. 7 shows the behavior of the two tests of decreasing current.

TABLE 4. Fourier series parameters for each current test.

Parameter	I_1	I_2	I_3	I_4	I_5
a_0	-19.04	32.77	11.82	-46.25	18.95
a_1	13.63	-15.56	-10.09	43.34	19.95
b_1	51.68	-34.61	-8.46	88.76	-0.7318
a_2	37.72	-16.86	-1.774	51.6	4.043
b_2	0.441	2.704	3.728	-37.99	-7.065
a_3	-1.204	-0.38	0	-19.5	-0.6949
b_3	-15.09	5.123	0	-14.5	-2.802
a_4	-3.911	0.3919	0	-0.4195	0
b_4	-0.7077	1.068	0	5.683	0
w	0.0192	0.0234	0.0282	0.0183	0.0275

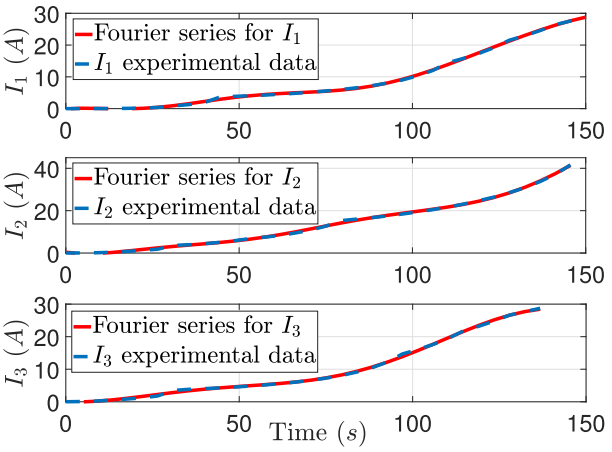

FIGURE 6. Behavior of Fourier series and current tests I_1, I_2, and I_3.

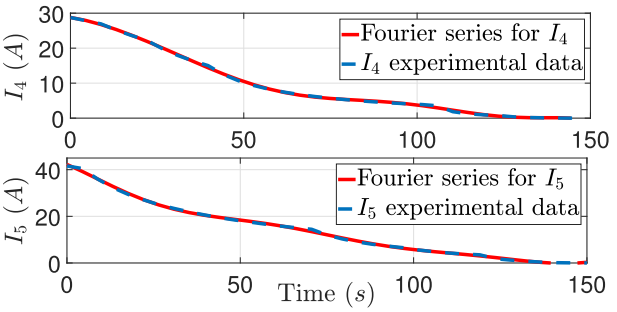

FIGURE 7. Behavior of Fourier series and current tests I_4 and I_5.

Taking into account the approximation of the electrical current of the PEMFC using the Fourier series, it is possible to calculate the analytical solution of the differential equations (4) and (5). Therefore, for each I_i, $\eta_{act,c,i} + \eta_{con,c,i}$ and $\eta_{act,a,i} + \eta_{con,a,i}$ are represented by the following time functions:

$$\left(\eta_{act,c,i} + \eta_{con,c,i}\right)(t) = A_0 \cdot \exp\left[\frac{-t}{\tau_c}\right] + \left(\frac{1}{C_c}\right) \cdot \left(a_{i,0} \cdot \tau_c + A_1 + A_2\right), \tag{12}$$

$$\left(\eta_{\text{act,a,i}} + \eta_{\text{con,a,i}}\right)(t) = B_0 \cdot \exp\left[\frac{-t}{\tau_\text{a}}\right] + \left(\frac{1}{C_\text{a}}\right) \cdot \left(a_{i,0} \cdot \tau_\text{a} + B_1 + B_2\right), \tag{13}$$

where the terms A_0, A_1, A_2, B_0, B_1, and B_2 are given by:

$$A_0 = \eta_{\text{act,c,i,0}} + \eta_{\text{con,c,i,0}} - \left(\frac{1}{C_\text{c}}\right) \cdot \left(a_{i,0} \cdot \tau_\text{c} + \sum_{j=1}^{4}\left(\frac{a_{i,j} \cdot \tau_\text{c} - j \cdot w_i \cdot \tau_\text{c}^2}{1 + (j \cdot w_i \cdot \tau_\text{c})^2}\right)\right), \tag{14}$$

$$A_1 = \sum_{j=1}^{4}\left(\frac{a_{i,j}}{1 + (j \cdot w_i \cdot \tau_\text{c})^2}\right) \cdot (\tau_\text{c} \cdot \cos[j \cdot w_i \cdot t] + j \cdot w_i \cdot \tau_\text{c}^2 \cdot \sin[j \cdot w_i \cdot t]), \tag{15}$$

$$A_2 = \sum_{j=1}^{4}\left(\frac{b_{i,j}}{1 + (j \cdot w_i \cdot \tau_\text{c})^2}\right) \cdot (\tau_\text{c} \cdot \sin[j \cdot w_i \cdot t] - j \cdot w_i \cdot \tau_\text{c}^2 \cdot \cos[j \cdot w_i \cdot t]), \tag{16}$$

$$B_0 = \eta_{\text{act,a,i,0}} + \eta_{\text{con,a,i,0}} - \left(\frac{1}{C_\text{a}}\right) \cdot \left(a_{i,0} \cdot \tau_\text{a} + \sum_{j=1}^{4}\left(\frac{a_{i,j} \cdot \tau_\text{a} - j \cdot w_i \cdot \tau_\text{a}^2}{1 + (j \cdot w_i \cdot \tau_\text{a})^2}\right)\right), \tag{17}$$

$$B_1 = \sum_{j=1}^{4}\left(\frac{a_{i,j}}{1 + (j \cdot w_i \cdot \tau_\text{a})^2}\right) \cdot (\tau_\text{a} \cdot \cos[j \cdot w_i \cdot t] + j \cdot w_i \cdot \tau_\text{a}^2 \cdot \sin[j \cdot w_i \cdot t]), \tag{18}$$

$$B_2 = \sum_{j=1}^{4}\left(\frac{b_{i,j}}{1 + (j \cdot w_i \cdot \tau_\text{a})^2}\right) \cdot (\tau_\text{a} \cdot \sin[j \cdot w_i \cdot t] - j \cdot w_i \cdot \tau_\text{a}^2 \cdot \cos[j \cdot w_i \cdot t]), \tag{19}$$

where $\eta_{\text{act,c,i,0}}+\eta_{\text{con,c,i,0}}$ and $\eta_{\text{act,a,i,0}}+\eta_{\text{con,a,i,0}}$ are the initial activation and concentration voltages for the cathode and anode for I_i, respectively. These voltages are calculated using (20).

$$\eta_{\text{act,i,0}} + \eta_{\text{con,i,0}} = V_\text{ini} - R_\text{mem} \cdot I_i(0) - V_{\text{fc},i}(0), \tag{20}$$

where

$$\eta_{\text{act,i,0}} + \eta_{\text{con,i,0}} = \eta_{\text{act,c,i,0}} + \eta_{\text{con,c,i,0}} + \eta_{\text{act,a,i,0}} + \eta_{\text{con,a,i,0}}. \tag{21}$$

From this result, the parameters of (10) were calculated (i.e. the parameters V_ini, R_mem, C_c, C_a, τ_c, and τ_a). Due to the monotonic behavior of the polarization curve, it was estimated $V_\text{ini} = \max[V_\text{fc}]$ (i.e. the maximum experimental voltage obtained, $V_\text{ini} = V_\text{fc}(0)$ for increasing current tests and $V_\text{ini} = V_\text{fc}(t_f)$ for decreasing current tests, where t_f is the final time of the test). Besides, to facilitate the construction of the electronic circuit, the capacitors must be equal, so it is assumed that $C_\text{c} = C_\text{a}$.

To calculate the parameters R_mem and C_c, a script was developed using MATLAB® software. The script and the MATLAB command *lsqcurvefit* (based on the least-square regression algorithm) were applied to adjust the parameters of the model to the voltage data obtained experimentally for the different electrical current tests. The values obtained were $R_\text{mem} = 0.50781\ \Omega$, and $C_\text{c} = 1.8857\ F$.

According to the references [55], [56], and [57], τ_c and τ_a are dependent on voltage and current. However, as a result of the script implementation, the values obtained for τ_c and τ_a were estimated as functions that only depend on the PEMFC voltage as follows.

$$\tau_\text{c} = 0.61 \cdot \exp\left[-\left(\frac{V_\text{fc} - 37.48}{1.689}\right)^2\right], \tag{22}$$

$$\tau_\text{a} = 0.832 \cdot \exp\left[-\left(\frac{V_\text{fc} - 35.75}{7.172}\right)^2\right]. \tag{23}$$

In the next section, parameters estimation is used to validate the proposed model through a comparison of the numerical simulations with experimental results.

V. EXPERIMENTAL VALIDATION AND DISCUSSION

A. SIMULATION AND RESULTS

To assess the effectiveness of the model in reproducing the real behavior of the PEMFC voltage, the relative error E_r, the mean error E_m, the mean squared error MSE, and the root mean square error $RMSE$ were calculated for all different experimental tests as follows.

$$E_\text{r} = \left(\frac{100}{N_\text{d}}\right) \cdot \sum_{\text{k}=1}^{N_\text{d}}\left|\frac{V_{\text{exp,k}} - V_{\text{sim,k}}}{V_{\text{exp,k}}}\right|, \tag{24}$$

$$E_\text{m} = \left(\frac{1}{N_\text{d}}\right) \cdot \sum_{\text{k}=1}^{N_\text{d}}\left|V_{\text{exp,k}} - V_{\text{sim,k}}\right|, \tag{25}$$

$$MSE = \left(\frac{1}{N_\text{d}}\right) \cdot \sum_{k=1}^{N_d}\left(V_{\text{exp,k}} - V_{\text{sim,k}}\right)^2, \tag{26}$$

$$RMSE = \sqrt{MSE}, \tag{27}$$

where N_d is the number of experimental data, $V_{\text{exp,k}}$ is the k experimental measurement (V), and $V_{\text{sim,k}}$ is the k simulation data from the model (V).

In Fig. 8 and 9, a comparison of numerical simulations of the proposed model with experimental results is shown. Increasing current tests were used for the comparison shown

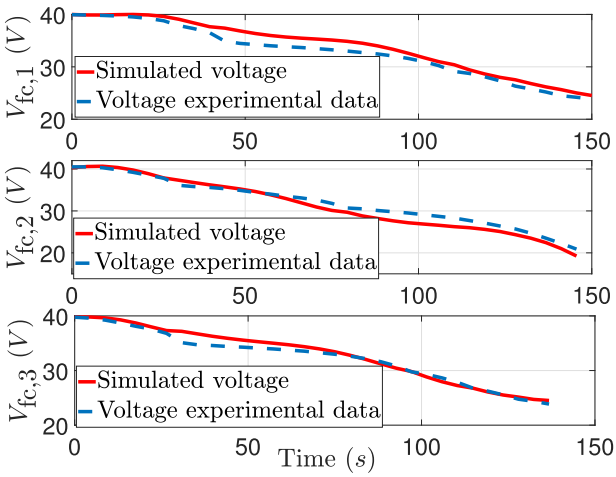

FIGURE 8. Behavior and comparison of the model with the experimental data for current tests I_1, I_2, and I_3.

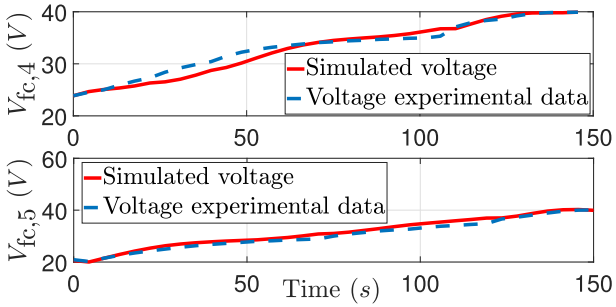

FIGURE 9. Behavior and comparison of the model with the experimental data for current tests I_4 and I_5.

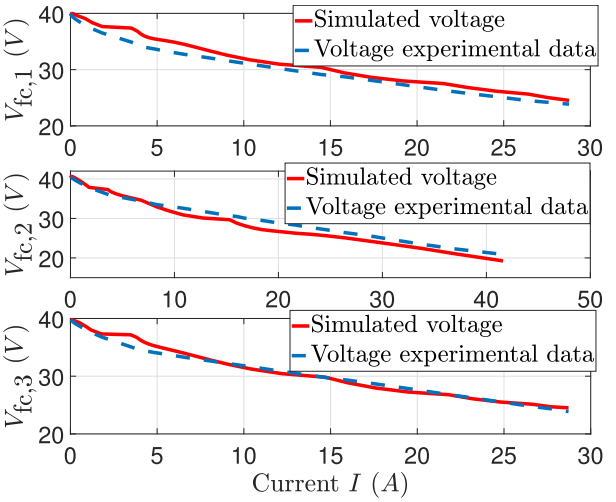

FIGURE 10. Behavior of the voltage-current model for current tests I_1, I_2, and I_3.

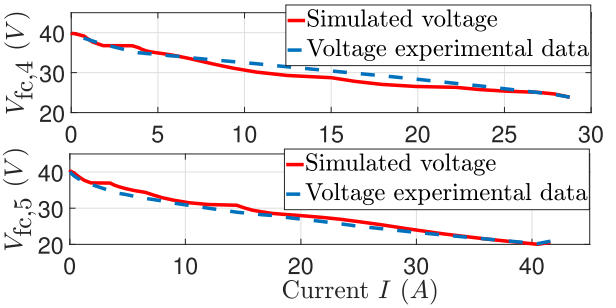

FIGURE 11. Behavior of the voltage-current model for current tests I_4 and I_5.

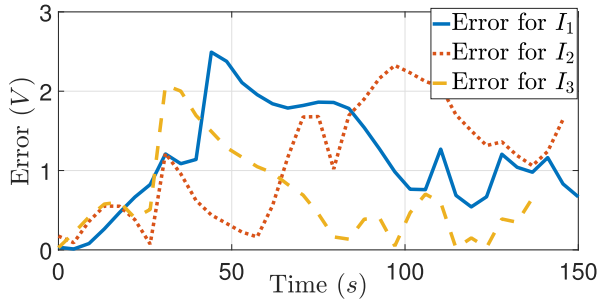

FIGURE 12. Behavior of the error obtained for current tests I_1, I_2, and I_3.

in Fig. 8. In this case, Test 1 had the most significant errors of the statistical tests (i.e., $E_r = 3.81\%$, $E_m = 1.442\ V$, $MSE = 1.7264\ V^2$, and $RMSE = 1.3139\ V$). This result in the statistical tests demonstrated the effectiveness of the model as a function of time in increasing currents.

In Fig. 9, the results obtained through numerical simulations and experimental tests have been compared for the decreasing current tests. In this comparison, Test 5 had the most significant errors of the statistical tests (i.e., $E_r = 3.15\%$, $E_m = 0.9496\ V$, $MSE = 1.2031\ V^2$, and $RMSE = 1.0969\ V$). This result in the statistical tests demonstrated the effectiveness of the model as a function of time in decreasing currents.

The behavior of the voltage-current model is shown in Fig. 10 and 11. A comparison of numerical simulations of the proposed model with experimental results is reported in Fig. 10. In this comparison, the V-I behavior of the experimental and simulation data can be observed when the input current increases. As can be seen, the PEMFC voltage drops when the PEMFC current increases.

In Fig. 11, a comparison of numerical simulations of the proposed model with experimental results is reported. In this case, the V-I behavior of the experimental and simulation data can be observed when the input current decreases. As can be seen, the PEMFC voltage increases when the PEMFC current drops.

Finally, the behavior of the error is shown in Fig. 12 and 13, for increasing and decreasing current tests, respectively. As can be seen in both figures, the errors obtained vary between 2.4923 V and 0.050 V. In addition, these errors as a function of time have a random behavior, which increases the difficulty to be modeled analytically. Therefore, applying control theory to minimize the errors obtained is a promising line of research to be addressed as future work.

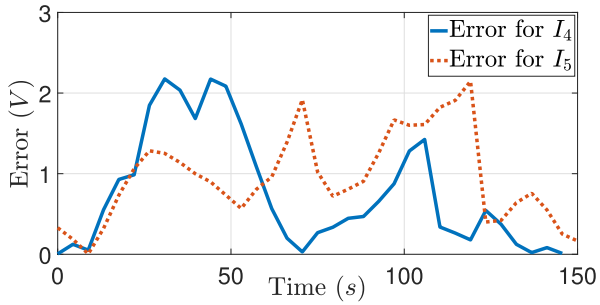

FIGURE 13. Behavior of the error obtained for current tests I_4 and I_5.

TABLE 5. Values of the maximum and minimum errors for each test.

Test	max	min
I_1	2.4923 V	0.0112 V
I_2	2.3251 V	0.0730 V
I_3	2.0758 V	0.0217 V
I_4	2.1754 V	0.0050 V
I_5	2.1460 V	0.0053 V

B. DISCUSSION

As mentioned at the beginning of this section, different tests were carried out to demonstrate the effectiveness of the model. In Tables 5 and 6, the results of the previous subsection are summarized. Table 5 shows the maximum and minimum error values obtained and Table 6 presents the mean, relative mean squared, and root mean square errors. From Table 5, it can be noted that the maximum and minimum errors for the five current tests were for I_1 with a value of 2.4923 V and I_4 with a value of 0.0050 V, respectively. According to Table 6, the mean error, I_1 had the maximum E_{m} with a value of 1.1442 V and I_3 had the minimum E_{m} with a value of 0.6549 V. In the case of relative error, I_2 had the maximum E_{r} with a value of 3.81% and I_3 had the minimum E_{r} with a value of 1.98%. Finally, the tests I_1 and I_3 obtained the maximum and minimum relative mean squared and root mean square errors with values of $MSE = 1.7264\ V^2$, $RMSE = 1.3139\ V$ and $MSE = 0.7292\ V^2$, $RMSE = 0.8539\ V$, respectively. It is also worth mentioning that the average value E_{m} and E_{r} of the five current tests were 0.92376 V and 2.984%, respectively.

Therefore, the developed ECM in this work is effective in describing the behavior of PEMFC voltage with different current inputs, both increasing and decreasing currents. Furthermore, using this model and the value of its parameters as a base, it is possible to build an electronic circuit that describes the behavior of Voltage PEMFC and replace the real PEMFC (i.e., construct a PEMFC emulator). However, the estimation of the model parameters is not optimal, and errors between the experimental data and the model can be observed. Besides, the obtained errors are particularly noticeable during the transient phenomena, which are complex to model according to the input current. Thus, taking into account the behavior of the transient phenomenon, it is possible to increase the reliability of the ECM for PEMFC voltage.

TABLE 6. Results of the statistical tests applied.

Test	E_{m}	E_{r}	MSE	$RMSE$
I_1	1.1442 V	3.58%	1.7264 V^2	1.3139 V
I_2	1.1102 V	3.81%	1.7131 V^2	1.3089 V
I_3	0.6549 V	1.98%	0.7292 V^2	0.8539 V
I_4	0.7599 V	2.40%	1.0779 V^2	1.0382 V
I_5	0.9496 V	3.15%	1.2031 V^2	1.0969 V

VI. CONCLUSION

In this work, the behavior of PEMFC voltage was investigated to develop an accurate dynamic-static ECM. Experimental tests allow identifying the dynamics of the PEMFC voltage for different input currents, both increasing and decreasing. The ECM was developed using five different current tests, three tests of increasing currents and two tests of decreasing currents. To complete the model, the parameters were estimated as constants, except for τ_{c} and τ_{a}, which were estimated as voltage-dependent functions. This new expression for τ_{c} and τ_{a} enriches previous works, where the authors only approximated these parameters as functions dependent on current and voltage.

The precision of the model was validated through different experimental tests, obtaining a mean relative error of 2.984%. The effectiveness of the ECM is illustrated through different experimental tests involving monotonic currents. For future work, testing the effectiveness of the model using currents with non-monotonic behavior would complement this work.

With the ECM developed in this work, different mathematical tools can be applied to improve the performance and optimize the PEMFC, for instance, the design and implementation of a control law. Besides, using the ECM and the calculated parameters, it is possible to build an electronic circuit for PEMFC voltage emulation, thus avoiding the use of a real PEMFC, which brings advantages in various research stages of PEMFC systems.

ACKNOWLEDGMENT

The authors would like to thank Dr. Luis H. Diaz-Saldierna from IPICYT and M. S. Carlo A. Beltran from the School of Sciences-UASLP, for their invaluable contributions in the experimental aspect.

REFERENCES

[1] A. Albarbar and M. Alrweq, *Introduction and Background*. Cham, Switzerland: Springer, 2018, pp. 1–8.
[2] K. Sopian and W. R. Wan Daud, "Challenges and future developments in proton exchange membrane fuel cells," *Renew. Energy*, vol. 31, no. 5, pp. 719–727, Apr. 2006.
[3] J. T. Pukrushpan, A. G. Stefanopoulou, and H. Peng, *Background and Introduction*. London, U.K.: Springer, 2004, pp. 1–13.
[4] J. Larminie and A. Dicks, *Introduction*. Hoboken, NJ, USA: Wiley, 2003, pp. 1–24.

[5] S. Barhate and R. Mudhalwadkar, "Portable fuel cell system emulator as a hardware-in-loop setup," in *Proc. Int. Conf. Commun. Inf. Process. (ICCIP)*, 2020, pp. 1–8.

[6] W. R. W. Daud, R. E. Rosli, E. H. Majlan, S. A. A. Hamid, R. Mohamed, and T. Husaini, "PEM fuel cell system control: A review," *Renew. Energy*, vol. 113, pp. 620–638, Dec. 2017.

[7] N. H. Jawad, A. A. Yahya, A. R. Al-Shathr, H. G. Salih, K. T. Rashid, S. Al-Saadi, A. A. AbdulRazak, I. K. Salih, A. Zrelli, and Q. F. Alsalhy, "Fuel cell types, properties of membrane, and operating conditions: A review," *Sustainability*, vol. 14, no. 21, p. 14653, Nov. 2022.

[8] L. Mao, L. Jackson, W. Huang, Z. Li, and B. Davies, "Polymer electrolyte membrane fuel cell fault diagnosis and sensor abnormality identification using sensor selection method," *J. Power Sources*, vol. 447, Jan. 2020, Art. no. 227394.

[9] F. Kartal and U. Özveren, "Investigation of an integrated circulating fluidized bed gasifier/steam turbine/proton exchange membrane (PEM) fuel cell system for torrefied biomass and modeling with artificial intelligence approach," *Energy Convers. Manage.*, vol. 263, Jul. 2022, Art. no. 115718.

[10] K. M. Bagherabadi, S. Skjong, and E. Pedersen, "Dynamic modelling of PEM fuel cell system for simulation and sizing of marine power systems," *Int. J. Hydrogen Energy*, vol. 47, no. 40, pp. 17699–17712, May 2022.

[11] Y. Qin, S. Ma, Y. Chang, Y. Liu, Y. Yin, J. Zhang, Z. Liu, K. Jiao, and Q. Du, "Modeling the membrane/CL delamination with the existence of CL crack under RH cycling conditions of PEM fuel cell," *Int. J. Hydrogen Energy*, vol. 46, no. 12, pp. 8722–8735, 2021.

[12] S. Gößling, N. Nickig, and M. Bahr, "2-D + 1-D PEM fuel cell model for fuel cell system simulations," *Int. J. Hydrogen Energy*, vol. 46, no. 70, pp. 34874–34882, Oct. 2021.

[13] A. Omran, A. Lucchesi, D. Smith, A. Alaswad, A. Amiri, T. Wilberforce, J. R. Sodré, and A. G. Olabi, "Mathematical model of a proton-exchange membrane (PEM) fuel cell," *Int. J. Thermofluids*, vol. 11, Jan. 2021, Art. no. 100110.

[14] A. Kulikovsky, "Analytical model for PEM fuel cell concentration impedance," *J. Electroanal. Chem.*, vol. 899, Oct. 2021, Art. no. 115672.

[15] Z. Zhang, J. Zhang, S. Hu, and T. Zhang, "An effective equivalent stiffness model combined with equivalent beam model to predict the contact pressure distribution for a large PEM fuel cell stack," *Int. J. Hydrogen Energy*, vol. 48, no. 30, pp. 11431–11441, 2022.

[16] A. Kulikovsky, "A model–based analysis of PEM fuel cell distribution of relaxation times," *Electrochimica Acta*, vol. 429, Oct. 2022, Art. no. 141046.

[17] D. Bernhard, T. Kadyk, S. Kirsch, H. Scholz, and U. Krewer, "Model-assisted analysis and prediction of activity degradation in PEM-fuel cell cathodes," *J. Power Sources*, vol. 562, Apr. 2023, Art. no. 232771.

[18] Y. Li, Z. Zhou, X. Liu, and W.-T. Wu, "Modeling of PEM fuel cell with thin MEA under low humidity operating condition," *Appl. Energy*, vol. 242, pp. 1513–1527, May 2019.

[19] K. J. Runtz and M. D. Lyster, "Fuel cell equivalent circuit models for passive mode testing and dynamic mode design," in *Proc. Can. Conf. Electr. Comput. Eng.*, 2005, pp. 794–797.

[20] D. Yu and S. Yuvarajan, "Electronic circuit model for proton exchange membrane fuel cells," *J. Power Sources*, vol. 142, nos. 1–2, pp. 238–242, Mar. 2005.

[21] J. Garnier, M. C. Pera, D. Hissel, F. Harel, D. Candusso, N. Glandut, J. P. Diard, A. De Bernardinis, J. M. Kauffmann, and G. Coquery, "Dynamic PEM fuel cell modeling for automotive applications," in *Proc. IEEE 58th Veh. Technol. Conf.*, Mar. 2003, pp. 3284–3288.

[22] W. Choi, J. W. Howze, and P. Enjeti, "Development of an equivalent circuit model of a fuel cell to evaluate the effects of inverter ripple current," *J. Power Sources*, vol. 158, no. 2, pp. 1324–1332, Aug. 2006.

[23] Z. Zhang, X. Huang, J. Jiang, and B. Wu, "An improved dynamic model considering effects of temperature and equivalent internal resistance for PEM fuel cell power modules," *J. Power Sources*, vol. 161, no. 2, pp. 1062–1068, Oct. 2006.

[24] W. Choi, P. N. Enjeti, and J. W. Howze, "Development of an equivalent circuit model of a fuel cell to evaluate the effects of inverter ripple current," in *Proc. 19th Annu. IEEE Appl. Power Electron. Conf. Expo.*, vol. 1, Oct. 2004, pp. 355–361.

[25] J. R. J. Larminie, "Current interrupt techniques for circuit modelling," in *Proc. IEE Colloq. Electrochem. Meas.*, 1994, pp. 12-1–12-6.

[26] M. J. Khan and M. T. Iqbal, "Modelling and analysis of electro-chemical, thermal, and reactant flow dynamics for a PEM fuel cell system," *Fuel Cells*, vol. 5, no. 4, pp. 463–475, Dec. 2005.

[27] J. M. Correa, F. A. Farret, V. A. Popov, and M. G. Simoes, "Sensitivity analysis of the modeling parameters used in simulation of proton exchange membrane fuel cells," *IEEE Trans. Energy Convers.*, vol. 20, no. 1, pp. 211–218, Mar. 2005.

[28] D.-J. Lee and L. Wang, "Dynamic and steady-state performance of PEM fuel cells under various loading conditions," in *Proc. IEEE Power Eng. Soc. Gen. Meeting*, Jun. 2007, pp. 1–8.

[29] E. Laffly, M.-C. Pera, and D. Hissel, "Dynamic model of a polymer electrolyte fuel cell power device," in *Proc. 32nd Annu. Conf. IEEE Ind. Electron.*, Nov. 2006, pp. 466–471.

[30] S. Page, S. Krumdieck, and A. Al-Anbuky, "Testing procedure for passive fuel cell state of health," in *Proc. Australas. Universities Power Eng. Conf.*, 2004, pp. 1–6.

[31] X. Qingshan, W. Nianchun, K. Ichiyanagi, and K. Yukita, "PEM fuel cell modeling and parameter influences of performance evaluation," in *Proc. 3rd Int. Conf. Electr. Utility Deregulation Restructuring Power Technol.*, Apr. 2008, pp. 2827–2832.

[32] K. P. Adzakpa, K. Agbossou, Y. Dube, M. Dostie, M. Fournier, and A. Poulin, "PEM fuel cells modeling and analysis through current and voltage transient behaviors," *IEEE Trans. Energy Convers.*, vol. 23, no. 2, pp. 581–591, Jun. 2008.

[33] J. M. Andújar, F. Segura, and M. J. Vasallo, "A suitable model plant for control of the set fuel cell–DC/DC converter," *Renew. Energy*, vol. 33, no. 4, pp. 813–826, Apr. 2008.

[34] S. Lazarou, E. Pyrgioti, and A. T. Alexandridis, "A simple electric circuit model for proton exchange membrane fuel cells," *J. Power Sources*, vol. 190, no. 2, pp. 380–386, May 2009.

[35] C. Brunetto, A. Moschetto, and G. Tina, "PEM fuel cell testing by electrochemical impedance spectroscopy," *Electr. Power Syst. Res.*, vol. 79, no. 1, pp. 17–26, Jan. 2009.

[36] C. Restrepo, C. Torres, J. Calvente, R. Giral, and R. Leyva, "Simulator of a PEM fuel-cell stack based on a dynamic model," in *Proc. 35th Annu. Conf. IEEE Ind. Electron.*, Nov. 2009, pp. 2796–2801.

[37] S. V. Puranik, A. Keyhani, and F. Khorrami, "State-space modeling of proton exchange membrane fuel cell," *IEEE Trans. Energy Convers.*, vol. 25, no. 3, pp. 804–813, Sep. 2010.

[38] R. Ferrero, M. Marracci, M. Prioli, and B. Tellini, "Simplified model for evaluating ripple effects on commercial PEM fuel cell," *Int. J. Hydrogen Energy*, vol. 37, no. 18, pp. 13462–13469, Sep. 2012.

[39] A. A. Fardoun, H. A. N. Hejase, A. Al-Marzouqi, and M. Nabag, "Electric circuit modeling of fuel cell system including compressor effect and current ripples," *Int. J. Hydrogen Energy*, vol. 42, no. 2, pp. 1558–1564, Jan. 2017.

[40] A. Mohammadi, G. Cirrincione, A. Djerdir, and D. Khaburi, "A novel approach for modeling the internal behavior of a PEMFC by using electrical circuits," *Int. J. Hydrogen Energy*, vol. 43, no. 25, pp. 11539–11549, Jun. 2018.

[41] T. Lan and K. Strunz, "Modeling of multi-physics transients in PEM fuel cells using equivalent circuits for consistent representation of electric, pneumatic, and thermal quantities," *Int. J. Electr. Power Energy Syst.*, vol. 119, Jul. 2020, Art. no. 105803.

[42] L. Baum, M. Schumann, F. Grumm, and D. Schulz, "Large-signal time-domain equivalent circuit model for PEM fuel cell stacks," *Int. J. Hydrogen Energy*, vol. 2023, pp. 1–12, Aug. 2023.

[43] M. Schumann, C. Cosse, D. Becker, D. Vorwerk, and D. Schulz, "Modeling and experimental parameterization of an electrically controllable PEM fuel cell," *Int. J. Hydrogen Energy*, vol. 46, no. 56, pp. 28734–28747, Aug. 2021.

[44] D. N. Avram, C. M. Davidescu, M. L. Dan, J. C. Mirza-Rosca, I. Hulka, E. M. Stanciu, and A. Pascu, "Corrosion resistance of NiCr(Ti) coatings for metallic bipolar plates," *Mater. Today, Proc.*, vol. 72, pp. 538–543, Jan. 2023.

[45] S. Laribi, K. Mammar, Y. Sahli, A. Necaibia, F. Z. Arama, and T. Ghaitaoui, "PEMFC water diagnosis using PWM functionality signal and fractional order model," *Energy Rep.*, vol. 7, pp. 4214–4221, Nov. 2021.

[46] N. Fouquet, C. Doulet, C. Nouillant, G. Dauphin-Tanguy, and B. Ould-Bouamama, "Model based PEM fuel cell state-of-health monitoring via AC impedance measurements," *J. Power Sources*, vol. 159, no. 2, pp. 905–913, Sep. 2006.

[47] Á. Hernández-Gómez, D. Langarica-Cordoba, P. R. Martinez-Rodriguez, D. Guilbert, V. Ramirez, and B. Saldivar, "PEM fuel cell emulators: A review," *Electronics*, vol. 12, no. 13, p. 2812, Jun. 2023.
[48] A. Albarbar and M. Alrweq, *Proton Exchange Membrane Fuel Cells: Review*. Cham, Switzerland: Springer, 2018, ch. 2, pp. 9–29.
[49] N. Benyahia, T. Rekioua, N. Benamrouche, and A. Bousbaine, "Fuel cell emulator for supercapacitor energy storage applications," *Electr. Power Compon. Syst.*, vol. 41, no. 6, pp. 569–585, Apr. 2013.
[50] Nexa Educational Packages. (2004). *Advanced Fuel Cell Learning Packages With a 1.2 kw Fuel Cell System*. [Online]. Available: https://paginas.fe.up.pt/ee00018/docs/Datasheet_Nexa.pdf
[51] J. T. Pukrushpan, A. G. Stefanopoulou, and H. Peng, *Fuel Cell System Model: Fuel Cell Stack*. London, U.K.: Springer, 2004, ch. 3, pp. 31–56.
[52] A. Gebregergis and P. Pillay, "Implementation of fuel cell emulation on DSP and dSPACE controllers in the design of power electronic converters," *IEEE Trans. Ind. Appl.*, vol. 46, no. 1, pp. 285–294, Jan. 2010.
[53] F. Musio, F. Tacchi, L. Omati, P. Gallo Stampino, G. Dotelli, S. Limonta, D. Brivio, and P. Grassini, "PEMFC system simulation in MATLAB-Simulink® environment," *Int. J. Hydrogen Energy*, vol. 36, no. 13, pp. 8045–8052, Jul. 2011.
[54] K. Sankar, K. Aguan, and A. K. Jana, "A proton exchange membrane fuel cell with an airflow cooling system: Dynamics, validation and nonlinear control," *Energy Convers. Manage.*, vol. 183, pp. 230–240, Mar. 2019.
[55] F. Gao, B. Blunier, M. G. Simões, and A. Miraoui, "PEM fuel cell stack modeling for real-time emulation in hardware-in-the-loop applications," *IEEE Trans. Energy Convers.*, vol. 26, no. 1, pp. 184–194, Mar. 2011.
[56] M. Cirrincione, M. C. Di Piazza, G. Marsala, M. Pucci, and G. Vitale, "Real time simulation of renewable sources by model-based control of DC/DC converters," in *Proc. IEEE Int. Symp. Ind. Electron.*, Jun. 2008, pp. 1548–1555.
[57] J. M. Correa, F. A. Farret, J. R. Gomes, and M. G. Simoes, "Simulation of fuel-cell stacks using a computer-controlled power rectifier with the purposes of actual high-power injection applications," *IEEE Trans. Ind. Appl.*, vol. 39, no. 4, pp. 1136–1142, Jul. 2003.

ÁNGEL HERNÁNDEZ-GÓMEZ received the Ph.D. degree in science from the Yucatan Scientific Research Center (CICY), Yucatán, Mexico, in 2022. He is currently a Postdoctoral Student with the School of Sciences, Universidad Autónoma de San Luis Potosí (UASLP), San Luis Potosí, Mexico. His current research interests include dynamic systems, control theory, and PEMFC and PEM electrolyzer modeling.

DIEGO LANGARICA-CORDOBA (Senior Member, IEEE) received the Ph.D. degree in engineering from Université de Paris-Sud XI, Orsay, France, in 2014. He is currently a Researcher with the School of Sciences, Autonomous University of San Luis Potosí (UASLP), San Luis Potosí, Mexico. His current research interests include nonlinear control theory, power conversion, renewable energy, and electric vehicles.

PANFILO R. MARTINEZ-RODRIGUEZ (Senior Member, IEEE) received the Ph.D. degree in applied science from Instituto Potosino de Investigación Cientifica y Tecnológica A.C. (IPICYT), San Luis Potosí, in 2007. From 2006 to 2016, he was a full-time Professor with Tecnológico Nacional de México (TecNM), Instituto Tecnológico Superior de Irapuato (ITESI), Mexico. Since 2017, he has been a Professor and a Researcher with Facultad de Ciencias, Universidad Autónoma de San Luis Potosí, Mexico. His current research interests include power electronics applications; the modeling, design, and control of power electronics converters applied to the improvement of the electrical power quality; and the electrical energy conversion from non-conventional electrical power sources.

DAMIEN GUILBERT was born in Paris, France, in 1987. He received the M.Sc. degree in electrical engineering and control systems and the Ph.D. degree in electrical engineering from the University of Technology of Belfort-Montiard (UTBM), France, in 2011 and 2014 respectively, and the H.D.R. degree in electrical engineering from the University of Lorraine, France, in June 2022. Since September 2016, he has been an Associate Professor with the University of Lorraine and a permanent member of the Group of Research in Electrical Engineering of Nancy (GREEN). His current research interests include power electronics for electrolyzer applications, proton exchange membrane electrolyzer modeling and emulation, and energy management of multi-source systems relying on renewable energy sources and hydrogen technologies.

VICTOR M. RAREZ-RIVERA received the M.Sc. degree from Centro de Investigación y de Estudios Avanzados del Instituto Politécnico Nacional, Mexico City, Mexico, in 2006, and the Ph.D. degree in engineering from Université de Paris-Sud XI-Supelec, Orsay, France, in 2014. He is currently a CONACYT Scientist with Centro de Investigación Científica de Yucatán (CICY), Unidad de Energía Renovable, Mérida, Mexico. His current research interests include renewable energy applications, hybrid systems, power electronics, non-linear control applications, and autonomous underwater vehicles.

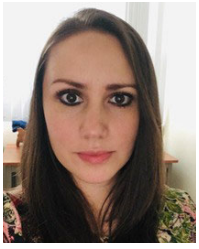

BELEM SALDIVAR received the B.S. degree in electronics and telecommunications engineering from the Autonomous University of Hidalgo State, UAEH, Mexico, in 2007, the M.Sc. degree in automatic control from the Center for Research and Advanced Studies of the National Polytechnic Institute (CINVESTAV), Mexico City, Mexico, in 2010, and the joint Ph.D. degree in automatic control from CINVESTAV and the Ph.D. degree in informatics and its applications from the Research Institute of Communication and Cybernetics of Nantes (IRCCyN), Nantes, France, in 2013. From 2014 to 2022, she was a Research Professor with the Catedras CONACyT Program, Faculty of Engineering, Autonomous University of the State of Mexico. Since 2022, she has been a full-time Professor with the Department of Automatic Control, CINVESTAV-IPN. Her current research interests include the modeling and control of (finite and infinite-dimensional) dynamic systems and nonlinear and time delay systems.